RESEARCH ARTICLE

Control of vortex on a non-slender delta wing by a nanosecond pulse surface dielectric barrier discharge

Guang-yin Zhao · Ying-hong Li · Hua Liang · Meng-hu Han · Wei-zhuo Hua

Abstract Wind tunnel experiments are conducted for improving the aerodynamic performance of delta wing using a leading-edge pulsed nanosecond dielectric barrier discharge (NS-DBD). The whole effects of pulsed NS-DBD on the aerodynamic performance of the delta wing are studied by balanced force measurements. Pressure measurements and particle image velocimetry (PIV) measurements are conducted to investigate the formation of leading-edge vortices affected by the pulsed NS-DBD, compared to completely stalled flow without actuation. Various pulsed actuation frequencies of the plasma actuator are examined with the freestream velocity up to 50 m/s. Stall has been delayed substantially and significant shifts in the aerodynamic forces can be achieved at the post-stall regions when the actuator works at the optimum reduced frequency of $F^+ = 2$. The upper surface pressure measurements show that the largest change of static pressure occurs at the forward part of the wing at the stall region. The time-averaged flow pattern obtained from the PIV measurement shows that flow reattachment is promoted with excitation, and a vortex flow pattern develops. The time-averaged locations of the secondary separation line and the center of the vortical region both move outboard with excitation.

List of symbols

c	Wing root chord length
x, y, z	Chordwise coordinate system
Re	Reynolds number based on the root chord length
f	Pulsed actuation frequency (Hz)

F^+	Reduced excitation frequency ($=fc/U_\infty$)
Cd	Drag force coefficient
Cl	Lift force coefficient
U_∞	Freestream velocity (m/s)
p	Static pressure on the model surface (Pa)
C_p	Pressure coefficient
V_{p-p}	Applied voltage to the plasma actuator (peak-to-peak) (kilovolt, kV)

Greek letters

α	Angle of attack (°)
Λ	Wing leading-edge sweep back angle (°)

Subscript

∞	Freestream condition

1 Introduction

For delta wings at low-to-moderate angles of attack, flow over the leading edge separates and forms shear layers that roll up into two primary large-scale vortexes which generate vortex lift. However, the nonlinear aerodynamic phenomena such as the vortex breakdown and the wake flow (large-scale flow separation) limit the flight regimes of aircraft with delta wings at high angles of attack. To improve the aerodynamic performance at high angles of attack, many investigations of vortical control techniques have been conducted by means of various passive and active devices, such as multiple vortices, control surfaces, blowing and suction, low-frequency and high-frequency excitation, feedback control, passive control with wing flexibility, and plasma actuators. These vortex control concepts employed for slender and non-slender delta

G. Zhao (✉) · Y. Li · H. Liang · M. Han · W. Hua
Science and Technology on Plasma Dynamics Laboratory,
Air Force Engineering University, Xi'an 710038,
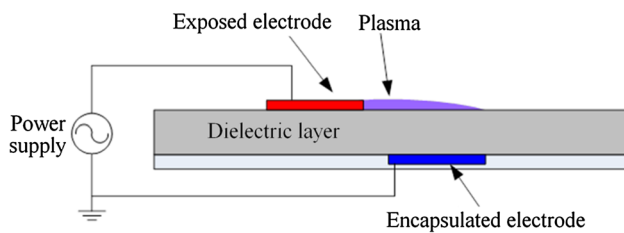People's Republic of China
e-mail: zym19860615@163.com

Exposed electrode   Plasma

Power
supply

Dielectric layer

Encapsulated electrode

Fig. 1 DBD plasma actuator

wings have been reviewed in the paper of Gursul et al. (2007).

Using plasma discharge actuators for flow control has been intensively investigated in the past decade, because of their attractive advantages compared with other techniques, such as very short response time, simple construction, low weights and sizes, wide-band control authority, low energy consumption, and the capability of closed loop feedback control. The recent developments in alternating current (AC)-DBD plasma actuator design and its novel applications for aerodynamic control have been reviewed in the paper of Wang et al. (2013). It has been demonstrated that AC-DBD can result in vortex stabilization (Sidorenko et al. 2013), delay the vortex breakdown onset over the delta wing surface (Kwak and Nelson 2010), produce roll maneuver, and provide longitudinal control for an unmanned air vehicle (UAV) wing (Patel et al. 2006; Nelson et al. 2007). As has been described and researched in many papers, the typical DBD plasma actuator used for flow separation control is depicted in Fig. 1.

Three arrangements of the plasma actuators are widely used in these investigations. Firstly, the DBD actuators are placed at the leading edge of wings, inducing an inward flow perpendicular to the leading edge. The aerodynamic improvements were obtained on a $\Lambda = 55°$ delta wing under this arrangement (Kwak and Nelson 2010). Also, the DBD plasma actuator of such arrangement was used to control leading-edge vortex on a semi-span delta wing ($\Lambda = 60°$) at typical micro-aerial vehicle Reynolds numbers, with the maximum Cl ($\alpha = 36°$) increased by 0.2 in the post-stall region at the optimum reduced frequency $F^+ = 1$ (Greenblatt et al. 2008). Secondly, the DBD actuators are placed at different chordwise locations, inducing downstream flows parallel to the leading edge. In the paper of Sidorenko et al. (2013), with DBD actuators placed perpendicularly to the leading edge across the vortex flow over a delta wing ($\Lambda = 65°$), high control efficiency was reached from the viewpoint of vortex breakdown. Another similar arrangement of plasma actuator inducing a wall jet downstream was used in the paper of Zhang et al. (2010). The aerodynamic improvements were obtained on delta wings ($\Lambda = 75°$) (Kwak and Nelson 2010; Zhang et al.

2010). Also, the effect of such DBD actuator on the vortical flow over a 75° swept flat-plate delta wing was investigated by Visbal and Gaitonde (2000), using simulated plasma actuators. With the actuator located near the apex, significant movement of the vortex breakdown location was demonstrated, and it was found to be more effective than the leading-edge or trailing-edge actuation. Thirdly, the DBD actuators are placed along the secondary separation line to affect the shear layer between the primary and the secondary vortices. Although such configuration was ineffective for delaying vortex breakdown, it proved to be effective from the viewpoint of vortex stabilization (Sidorenko et al. 2013).

These arrangements of plasma actuators are similar to that of the blowing and suction which are commonly used in three versions: (a) leading-edge blowing/suction (b) blowing from small aspect ratio jets (usually along the core or parallel to leading edge), and (c) trailing-edge blowing. However, the small velocity induced by plasma actuators limits its efficacy for flow control under higher freestream velocities. The maximal freestream velocity in prior tests is <20 m/s; hence, the corresponding Reynolds (Re) numbers are low.

To realize high-speed flow control, the nanosecond pulsed DBDs have been investigated in recent years. When pulsed nanosecond high voltage is applied on the electrodes, the air near the electrodes is weakly ionized following a local temperature rise and pressure rise in the vicinity of plasma region. The main mechanism is fast gas heating with very small induced flow velocity ($U_{max} \sim 0.5$ m/s), which is much different from that of AC-based DBD that mainly uses momentum forcing. As a new unsteady excitation method used for flow control, nanosecond dielectric barrier discharge (NS-DBD) has been used for leading-edge separation control on airfoil at Mach (Ma) number from 0.03 to 0.74 (Roupassov et al. 2009), for manipulation of strong shock wave ahead of an circular cylinder (Nishihara et al. 2011), plasma-assisted ignition, and high-speed flow control (Adamovich et al. 2009), and for leading-edge separation control at realistic takeoff and landing Re and Ma numbers (Rethmel et al. 2011).

The purpose of this study was to investigate the potential of NS-DBD for vortical flow control on a non-slender delta wing in the range of Re numbers higher than that has previously been investigated. To bring periodic perturbations, the plasma actuator was placed at the leading edge of the delta wing. Effect of NS-DBDs on the aerodynamic performance of the delta wing was studied by balanced force measurements in the wind tunnel. Also, pressure measurements and particle image velocimetry (PIV) measurements were conducted to investigate the formation of leading-edge vortices. At last, the control mechanism is discussed.

2 Experimental setup

2.1 Wind tunnel

The experiments were conducted in a low-speed wind tunnel in Air Force Engineering University. The wind tunnel is closed and recirculating with velocity ranging from 5 to 80 m/s. The test section of the tunnel is nominally 1.0 m high, 1.2 m wide, and 1.5 m long. The turbulence intensity of the freestream velocity is <1 %.

2.2 Experimental model

The model was designed seriously by referring to the previous active flow control investigations on delta wings. Gursul et al. (2007) suggested that for highly swept wings, reattachment on the wing surface does not occur beyond very small angles of attack and therefore is difficult to manipulate and that for non-slender wings, reattachment of

Fig. 2 Schematics of the delta wing model used in the experiments

the flow on the wing surface can be manipulated by active and passive control methods. For non-slender wings, perturbations introduced along leading edge have been demonstrated to have efficacy for vortical flow control (Patel et al. 2006; Williams et al. 2008; Kwak and Nelson 2010). Here, the model's sweep angle was set to 47°, the same used for the model in the paper of Patel et al. (2006). The dimension of the model was designed with consideration of the camera's field of view and the blockage ratio to the wind tunnel. At last, the model used is a delta wing with a leading-edge sweep angle of $\Lambda = 47°$, root chord length $c = 240$ mm, and thickness of 8 mm (Fig. 2). The model consists of a flat-plate delta wing and a cylinder center body with a diameter of 50 mm. The model was made of a dielectric material (Plexiglas), and the leading edge was beveled from both sides at 10 mm × 3.5 mm (Fig. 3a).

The model was attached to the internal balance that linked to the angle-adjusting mechanism in the wind tunnel test section through the cylinder center body. Maximum blockage in the current study is <3 % and occurs at $\alpha = 25°$. No blockage or wall corrections have been employed in the data processing.

2.3 DBD actuators and high-voltage equipment

The DBD actuator consists of electrodes, dielectric material, and voltage generation system, as has been described in Fig. 1. Copper is selected to be used for the DBD electrodes. It has a total thickness of 0.018 mm and is bonded with an acrylic adhesive that is 0.02 mm thick. The dielectric barrier was made of three layers of a Kapton adhesive film with a total thickness of 0.195 mm. Each tape has a silicon adhesive layer that is 0.04 mm thick. The effect of the silicon adhesive on the dielectric performance is not examined here. The covered electrode with a width of 10 mm was connected to the ground; the exposed electrode connected to the high-voltage generator was 3 mm wide. The two electrodes were glued to the barrier with a 0-mm inner-gap. The actuator was located at the leading edges lightly on the windward surface, in close
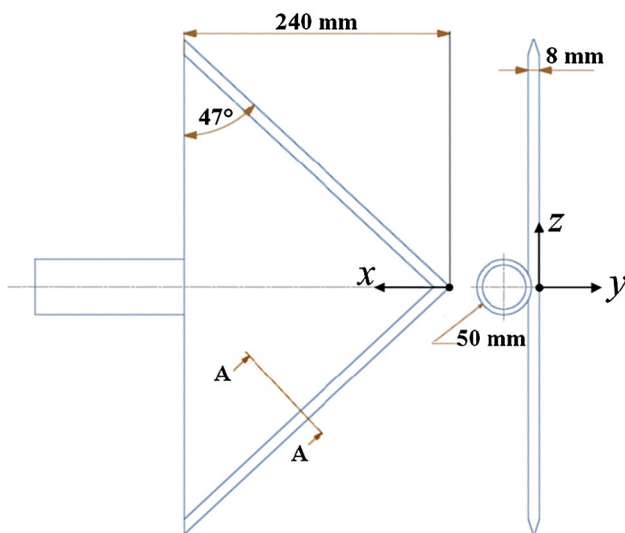
Fig. 3 Details of the plasma actuator arrangements (**a**) and the voltage and current pulses on the leading-edge DBD actuator ($V_{p-p} = 12$ kV, $f = 1,000$ Hz) (**b**)
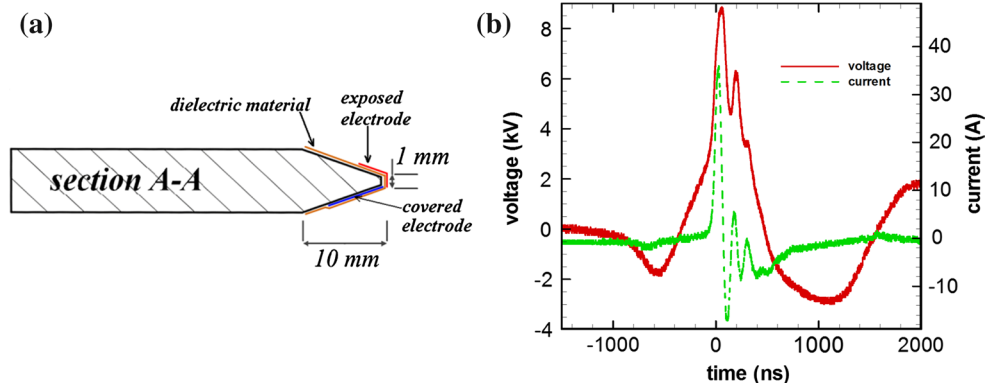
Table 1 Electrical properties of NS-DBD plasma on the 64-cm-long actuator applied at the leading edge of the model

F (Hz)	V_{p-p} (kV)	Energy (mJ/pulse)	Power (W)
200	≈12 kV	≈17.1	≈3.4
400	≈12 kV	≈16.2	≈6.5
600	≈12 kV	≈15.9	≈9.5
800	≈12 kV	≈15.8	≈12.6
1,000	≈12 kV	≈14.9	≈14.9

Fig. 4 Distribution of static pressure taps

proximity to the separation point, where proved to be most effective at high angles of attack in the paper of Patel et al. (2006). The electrodes overlap for almost the entire leading edge (≈64 cm). Figure 3a shows the details of the plasma actuators used in current research.

The DBD power supply was a nanosecond pulse generator capable of producing pulses of up to 80 kV of magnitude with rising time of 10–30 ns. Voltage and the current were measured by means of four-channel DPO4104 Tektronix oscilloscope, Tektronix P6015A high-voltage probe and a current probe (Tektronix TCP312 + TCPA300). An example of measured high voltage and current in 1 kHz is shown in Fig. 3b. The peak current in the discharge is 36 A, and peak powers of up to 300 kW are created. While this power is exceptionally high due to the short pulse width and high current, the average power for the NS-DBD is slightly low due to its much higher duty cycle. Table 1 presents various electrical parameters for the NS-DBDs operating at different frequencies. The NS-DBD pulse energy is found to vary slightly with frequency.

3 Measurement techniques

3.1 Force measurements by balance

The time-averaged lift and drag forces of the model were measured by a six-component internal strain gauge balance. The yaw angle and the roll angle were 0° in all tests. The overall uncertainty in both the lift and the drag measurements were estimated <1 %, by repeating the force measurement of the calibration model (TN-4041) four times, which showed that the force measurements were stable and reliable. The cable interference and the electric–magnetic interference (EMI) from the plasma actuator system would influence the force measurements. Those interferences were eliminated by the refinement of the wind tunnel test procedure, and by the grounding and shielding of the electric equipment.

3.2 Pressure measurements system

Measurements of static pressure are acquired from taps on the model surface using Scanivalve digital pressure sensor
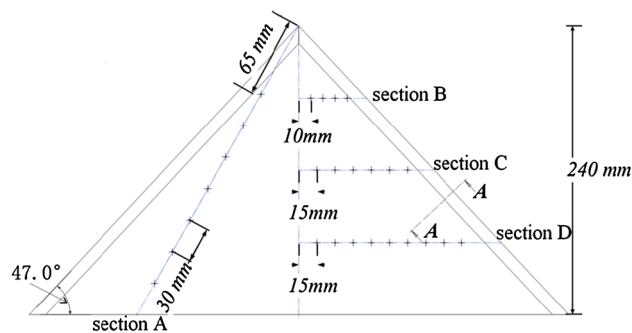
arrays (DSY-JB2008), with a pressure range of −11 to 11 kPa. The right upper surface of the wing was designed with 19 static pressure taps positioned at three streamwise stations, corresponding to $x/c = 0.25$ (station B), $x/c = 0.50$ (station C), and $x/c = 0.75$ (station D), respectively. The left upper surface was designed with seven static pressure taps along the 60 % spanwise stations. The locations of these taps are shown in Fig. 4 by the symbol of asterisk on the wing surface. Samples were taken at 100 Hz, and each tap was measured for 6 s.

The static pressure measured by the electrical pressure transducer was normalized using the following equation.

$$C_p = \frac{p - p_\infty}{\frac{1}{2} \rho_\infty U_\infty^2}$$

where C_p is the coefficient of static pressure and p is the measured static pressure on the wing surface. The uncertainty of the pressure measurements by such traditional pressure tap technique was estimated to be <2 % for the present flow conditions.

3.3 2-D velocity measurements by PIV

In addition to force measurements and static pressure measurements, 2-D PIV was performed above the model's upper surface at location $x/c = 0.35$ for the optimum control case. The PIV measurement plane was normal to the surface and root chordline. Measurements were made with two Nd:YAG 100-mJ lasers and a 1,024 × 1,024 pixel CCD camera. The CCD camera used to capture the particle images was installed on the pylon downstream of the model, so the plane of measurements was always normal to the model's surface. The layout of the PIV measurement is shown in Fig. 5. A commercial seed-particle generator was used to generate particles with an average diameter of 1 μm. Because the wind tunnel is a return-flow tunnel, particle seeding was inserted from the rear of the model. In such way, the interference from the seed-particle generator to the flow field can be avoided and the particles can be mixed uniformly.
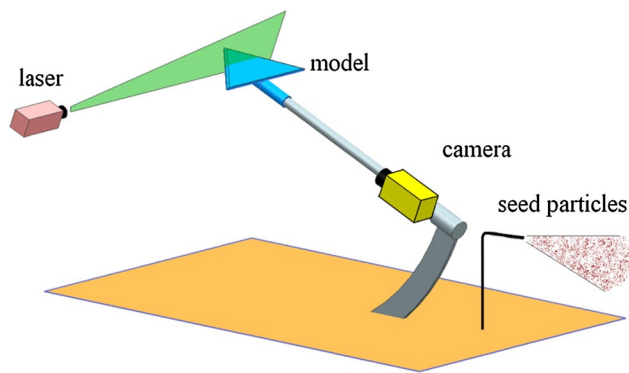
Fig. 5 Schematics of the wind tunnel test

Images were acquired and processed using a LaVision PIV system. For each image pair, subregions were cross-correlated using decreasing window size (64^2–32^2 pixel^2) multi-pass processing with 50 % overlap. The resulting velocity fields were post-processed to remove spurious vectors using an allowable vector range and median filter. Removed vectors were replaced using an interpolation scheme based on the average of neighboring vectors. A 3×3 Gaussian smoothing filter was also applied to the calculated velocity fields. Uncertainty of a single measurement was <2 % (for 20 m/s) and the percentage of spurious vectors never exceeded 3 %. The velocity field resolution of PIV was about 1.8 mm, sufficient to resolve the secondary separation and the vortex near the leading edge. The PIV data were sampled at 14 Hz. Time-averaged statistics of velocity distributions were obtained by pairs of 56 particle images for each test case.

Leading-edge vortical control studies were performed at primarily $Re = 0.72 \times 10^6$ (50 m/s) and 0.29×10^6 (20 m/s) based on the root chord length of the delta wing. Table 2 shows the test conditions of each measurement.

4 Results and discussion

As is common in most active flow control studies, the effect of the plasma-induced perturbation on the wing's aerodynamic performance was assessed by performing a range of

actuation frequency (200–1,000 Hz) at a series of angles of attack (0–25°). The applied peak-to-peak voltage V_{p-p} was fixed at 12 kV. The results for lift and drag coefficients for a range of attack angles are shown in Fig. 6a, b.

It can be seen that with the discharge on, the critical angle of attack and the maximum lift coefficient increased to different degrees under different actuation frequencies, when compared with the plasma off case. The corresponding reduced frequency F^+ was 1, 2, 3, and 5, respectively. From the tested cases, the optimum actuation frequency was $F^+ = 2$ ($f = 400$ Hz), with the critical angle of attack increased by approximately 4° and the post-stall lift coefficient increased by 14.7 % at $\alpha = 24°$. The effect of actuation on the drag coefficient was similar to the lift. Under actuation, the drag coefficient also increased for the vortex enhancement which will contribute to the increase in the induced drag.

In the paper of Greenblatt et al. (2008), unsteady AC-DBD was used for delta wing flow control and found that there was an optimum frequency range of $fc/U_\infty = 1$–2 for $Re = 75,000$. Here, we detected the optimum reduced frequency $F^+ = 2$ for $Re = 720,000$. Also, compared with the results in the paper of Patel et al. (2006), the data obtained in current force measurements demonstrated the high efficiency of NS-DBD for the leading-edge vortex control, compared with that of the AC-DBD.

Some understanding of the optimum reduced frequency can be gained from the analyses in the papers of Gursul et al. (2005) and (Gordnier and Visbal 2005), which suggested that the optimum range of frequencies are related to the dominant frequencies of the shear layer instabilities. The paper of Gursul et al. (2007) suggested that the unsteady excitation can excite the Kelvin–Helmholtz instability of the separated shear layer and promote reattachment.

The optimum frequency detected here are broadly consistent with other active flow control methods by introducing perturbations at the leading edge of delta wings, such as piezoelectric fluidic actuators (Margalit et al. 2005), pulsed blowing from the leading edge (Williams et al. 2008), and the unsteady AC-DBD actuators (Patel et al. 2006; Greenblatt et al. 2008).

According to the results of force measurements, the effect of NS-DBD on the time-averaged pressure

Table 2 Wind tunnel test conditions

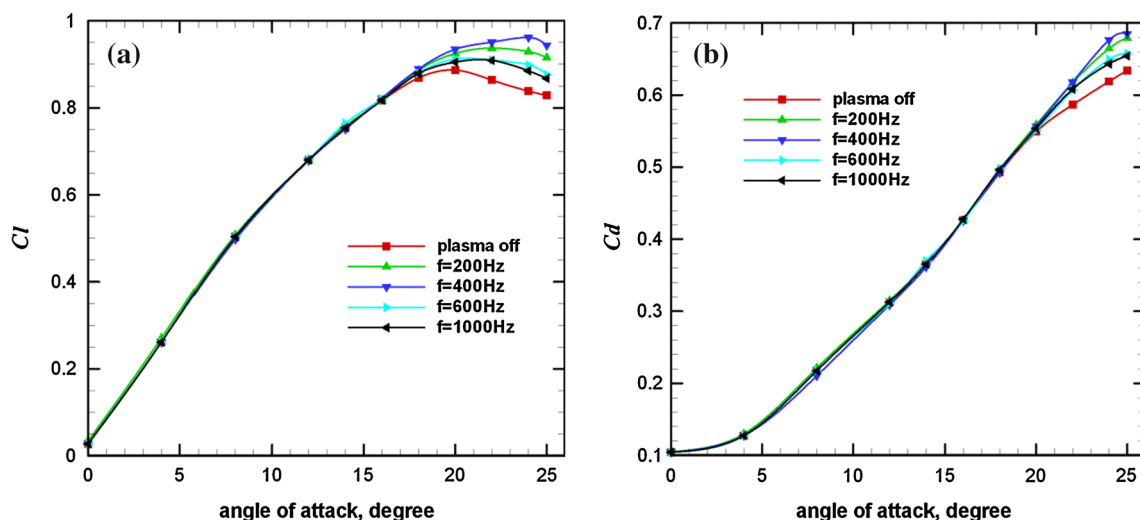| Measurement items	Force measurement	Pressure measurement	PIV measurement
α	0–25°	22°	22°
U_∞ (m/s)	50	50	20
Re	0.72×10^6	0.72×10^6	0.29×10^6
f (Hz)	200, 400, 600, 1,000	200, 400, 600, 800, 1,000	200, 300, 400
V_{p-p} (kV)	12	12	10.5

Fig. 6 Effects of plasma actuators on the lift coefficient (**a**) and drag coefficient (**b**) of the 47° swept delta wing for a range of angles of attack ($U_\infty = 50$ m/s)
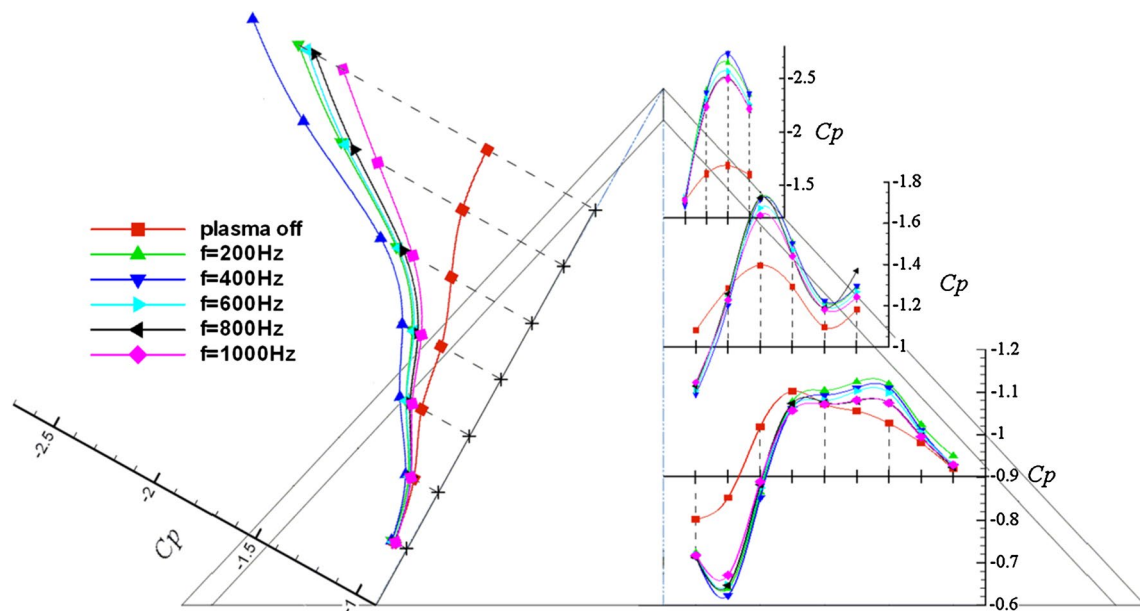

Fig. 7 Static pressure distributions on the upper surface of the delta wing under fixed values of freestream velocity $U_\infty = 50$ m/s and $\alpha = 22°$

distribution was investigated at $\alpha = 22°$ for the obvious control effect at this angle of attack. Figure 7 shows the static pressure distributions on the upper surface of the delta wing which are represented by the pressure coefficient. It can be seen that when the plasma was off, the static pressure of the upper surface had a very flat pressure distribution for the wing was stalled.

When the actuator was ignited, from the pressure distribution along the section A, B, and C, the well-defined suction peak was observed, especially near the apex. It indicated that the strong leading-edge vortex was formed for

the actuated cases. The flow control effects dependence on actuation frequency were consonant with the results from force measurements in Fig. 6. From the pressure distribution along the section A and D, it was found that the changes of C_p at the rearward were not as obvious as that of the forward part of the wing.

Due to the limited number of pressure taps, the position changes of vortex core and the secondary separation line cannot be observed from the pressure distribution obtained here. An attempt to gain understanding of the control mechanism was undertaken by performing 2-D PIV
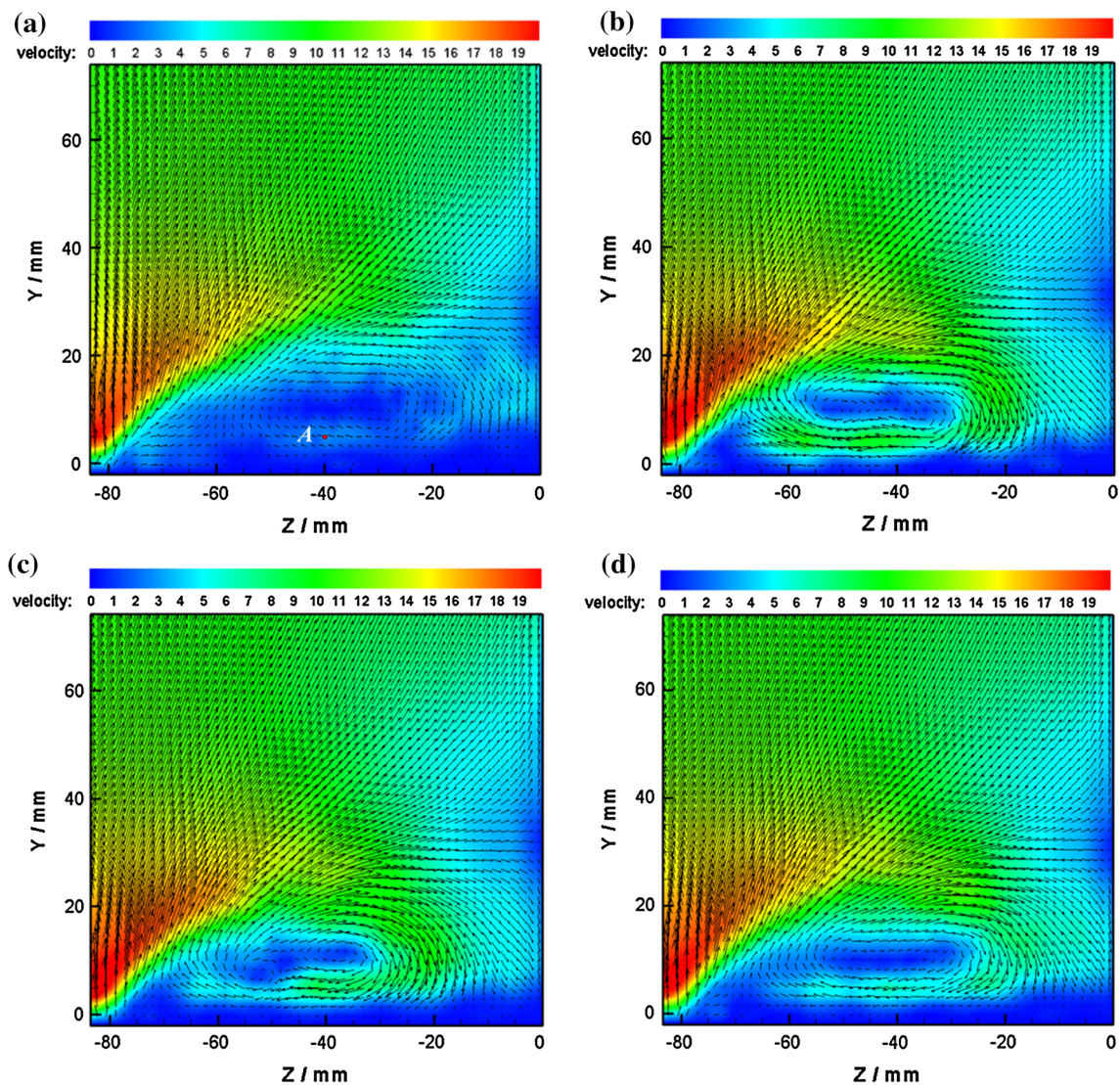
Fig. 8 Velocity distribution obtained by means of PIV ($U_\infty = 20$ m/s and $\alpha = 22°$) for the case with no excitation (**a**) and with DBD activated at $f = 200$ Hz ($V_{p-p} = 10.5$ kV) (**b**), 300 Hz ($V_{p-p} = 10.5$ kV) (**c**), 400 Hz ($V_{p-p} = 10.5$ kV) (**d**)

measurements in the y–z plane at $x/c = 0.35$ on the left part of the delta wing (see Fig. 5). Figure 8 shows the time-averaged velocity distributions at $\alpha = 22°$ by PIV technique. For the present case, the wing was well beyond its stall angle, and the separated flow formed a shear layer at the leading edge. In this deep stall state, almost no remnant of the leading-edge vortex remains (see Fig. 8a).

Velocity distributions with excitation at several frequencies in the section $x/c = 0.35$ are presented in Fig. 8b, c, d. PIV data confirmed that excitation to the vortical flow by leading-edge actuation was beneficial for the primary vortex reattachment and enhancement in the post-stall region. Firstly, with forcing, the center of the vortex flow pattern moved outboard, significantly further outboard of the plasma off case. Because

of complete reattachment, the attachment line and the secondary vortex separation line also moved outboard. Quantitative changes of the secondary separation line are shown in Table 3. Secondly, swirling velocity of the vortex was clearly increased compared with the plasma off case, which was responsible for the vortex enhancement resulting in the lift augment. Thirdly, the vortex structure was improved to different degrees under different excitation frequencies. The swirling velocities of point A ($x = -40$ mm, $y = 5$ mm) under different actuation frequencies are given in Table 4. For the tested PIV measurements, the swirling velocity of the vortex under excitation frequency of 200 Hz was higher.

Vortices that have undergone breakdown can be viewed as curved shear layers, and perturbations introduced along

Table 3 Secondary separation position in the measurement plane

Plasma off case	$f = 200$ Hz	$f = 300$ Hz	$f = 400$ Hz
$x = -57$ mm	$x = -71$ mm	$x = -70$ mm	$x = -69$ mm

Table 4 Swirling velocity at the point A ($x = -40$ mm, $y = 5$ mm)

Plasma off case	$f = 200$ Hz	$f = 300$ Hz	$f = 400$ Hz
3.0 m/s	9.3 m/s	8.1 m/s	6.1 m/s

the leading edge profoundly affect them, producing significant changes to the wing's normal force (Margalit et al. 2005; Greenblatt et al. 2008). The perturbations can be produced by leading-edge blowing and suction or unsteady mode of AC-DBD, which have been demonstrated their availability in vortical flow control over delta wings (Williams et al. 2008; Greenblatt et al. 2008; Kwak and Nelson 2010). From the viewpoint of perturbation, the NS-DBD with very small induced flow velocity can also produce forceful perturbations such as shock wave and induced vortex. The paper of Williams et al. (2008) utilized oscillatory blowing at the leading edge of a non-slender delta wing for vortical flow control. Phase-averaged measurements reveal the perturbation due to the pulsed blowing, its interaction with the shear layer and vortex, apparent displacement of the vortex core, and relaxation of the reattachment region. Here, the NS-DBD obtains the similar results. More detailed phase-averaged PIV data and analysis added insight into the mechanism about the leading-edge unsteady actuation (Greenblatt et al. 2008). It was suggested that the curved shear layer above the wing's surface could be strongly affected by the unsteady actuation produced by AC-DBDs. Some instantaneous flow patterns by PIV measurements may give some understanding of the flow control mechanism by NS-DBD actuator, as shown in Fig. 9.

It was believed that NS-DBD actuation in the vicinity of the separated point could induce spanwise vortex to the shear layer, in the flow control of 2-D airfoil (Rethmel et al. 2011). Here, for delta wing, when the plasma was on, a new vortex was formed near the leading edge, and this vortex will develop into a large one. The phenomena periodically continued during the actuation. It was supposed that the reforming of leading-edge vortex, resulted from periodic emanation of small-scale vortices moved along the shear layer due to the pulsed actuation, may be the mechanism.

Due to the relatively high flow speed (20 m/s), the effective actuation frequency of 200 Hz is really much higher than the sampling frequency (14 Hz) by the camera, so development of the induced vortex is hard to resolve. Also, the phase-averaged PIV measurements were not conducted in the present study. Hence, time history flow field measurements by the phase-locked technique are needed to valid the conclusions in future work.

5 Conclusions

Active flow control on a non-slender delta wing with sweep angle of $\Lambda = 47°$ at post-stall incidences was demonstrated by a pulsed NS-DBD from the leading edge. Force and pressure measurements were conducted to examine the whole effect of such unsteady excitation on the aerodynamic characteristic of the delta wing. In the experiments, the EMI noise from plasma actuator was successfully
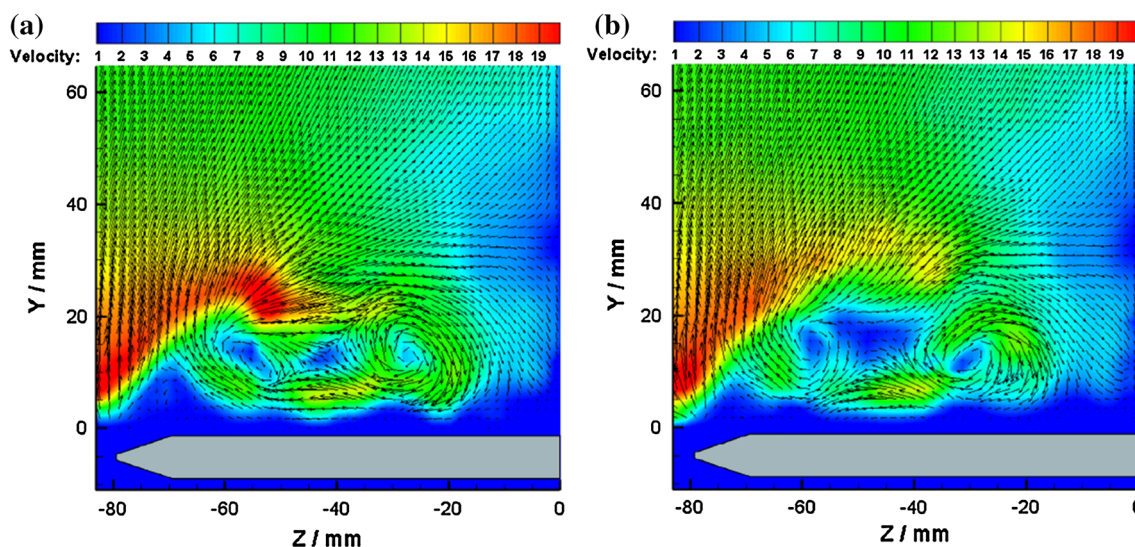
Fig. 9 Some instantaneous flow patterns by PIV measurements with DBD activated at $f = 200$ Hz ($V_{p-p} = 10.5$ kV)

shielded by the refinement of the test procedure; also the data from PIV measurements were processed elaborately. From these ways, uncertainty of the experimental measurement was reduced effectively. From the force measurements, it is clear that the pulsed NS-DBD actuation can significantly enhance the performance of the non-slender delta wing. The critical angle of attack is increased by approximately 4°, and the post-stall lift coefficient is increased by 14.7 % at $\alpha = 24°$, when the separated shear layer was excited at the optimum actuation frequency of $F^+ = 2$ ($f = 400$ Hz).

At a post-stall incidence angle with the actuator ignited, a flat pressure distribution changed into a pressure distribution with strong suction peak, indicating the formation of a vortex and the reattachment in the forward part of the wing. The trend of pressure changes versus actuation frequency was consonant with the force measurements by the balance.

Two-dimensional PIV measurements were performed to give an insight into the microscopic changes of vortex flow pattern under actuation in post-stall region. The flow pattern obtained from PIV measurements showed that flow reattachment was promoted under actuation, and a vortex flow pattern developed with swirling velocity in the vortex was clearly increased. The time-averaged location of the center of the vortical region moved outboard with excitation; the attachment line and the secondary vortex separation line also moved outboard.

References

Adamovich IV, Choi I, Jiang N, Kim J-H, Keshav S, Lempert WR, Mintusov E, Nishihara M, Samimy M, Uddi M (2009) Plasma assisted ignition and high-speed flow control: non-thermal and thermal effects. Plasma Sources Sci Technol 18:034018

Gordnier RE, Visbal MR (2005) Compact differences scheme applied to simulation of low-Sweep delta wing flow. AIAA J 43(8):1744–1752

Greenblatt D, Kastantin Y, Nayeri CN, Paschereit CO (2008) Delta-wing flow control using dielectric barrier discharge actuators. AIAA J 46(6):1554–1560

Gursul I, Gordnier R, Visbal M (2005) Unsteady aerodynamics of nonslender delta wings. Prog Aerosp Sci 41:515–557

Gursul I, Wang Z, Vardaki E (2007) Review of flow control mechanisms of leading-edge vortices. Prog Aerosp Sci 43:246–270

Kwak DY, Nelson RC (2010) Vortical flow control over delta wings with different sweep back angles using DBD plasma actuators. AIAA 2010-4837, 5th Flow Control Conference, Chicago, Illinois

Margalit S, Greenblatt D, Seifert A, Wygnanski I (2005) Delta wing stall and roll control using segmented piezoelectric fluidic actuators. J Aircr 42(3):698–709

Nelson RC, Corke TC, He C, Othman H, Matsuno T (2007) Modification of the flow structure over a UAV wing for roll control. AIAA 2007-884, 45th AIAA aerospace sciences meeting and exhibit, Reno, NV

Nishihara M, Takashima K, Rich JW, Adamovich IV (2011) Mach 5 bow shock control by a nanosecond pulse surface dielectric barrier discharge. Phys Fluids 23:066101

Patel MP, Ng TT, Vasudevan S, Corke TC, He C (2006) Plasma actuators for hingeless aerodynamic control of an unmanned air vehicle. AIAA 2006-3495, 3rd AIAA Flow Control Conference, San Francisco, California

Rethmel C, Little J, Takashima K, Sinha A, Adamovich I, Samimy M (2011) Flow separation control over an airfoil with nanosecond pulse driven DBD plasma actuators. AIAA 2011-487, 49th AIAA Aerospace Sciences Meeting including the New Horizons Forum and Aerospace Exposition, Orlando, Florida

Roupassov DV, Nikipelov AA, Nudnova MM, Starikovskii AY (2009) Flow separation control by plasma actuator with nanosecond pulsed-periodic discharge. AIAA J 47(1):168–185

Sidorenko AA, Budovskiy AD, Maslov AA, Postnikov BV, Zanin BY, Zverkov ID, Kozlov VV (2013) Plasma control of vortex flow on a delta wing at high angles of attack. Exp Fluids 54:1585

Visbal MR, Gaitonde DV (2000) Control of vortical flows using simulated plasma actuators. AIAA 2006-505, 44th AIAA Aerospace Sciences Meeting and Exhibit, Reno, Nevada

Wang JJ, Choi KS, Feng LH, Jukes TN, Whalley RD (2013) Recent developments in DBD plasma flow control. Prog Aerosp Sci 62:52–78

Williams NM, Wang Z, Gursul I (2008) Active flow control on a non-slender delta wing. AIAA 2008-740, 46th AIAA Aerospace Sciences Meeting and Exhibit, Reno, Nevada

Zhang PF, Wang JJ, Feng LH, Wang GB (2010) Experimental study of plasma flow control on highly swept delta wing. AIAA J 48(1):249–252